POLITECNICO DI TORINO
Repository ISTITUZIONALE

On durable materials for dielectric-barrier discharge plasma actuators

(Article begins on next page)

21 December 2024

On durable materials for dielectric-barrier discharge plasma actuators

Philipp Warlitz [a], Marc T. Hehner [a], Saskia Pasch [a], Jacopo Serpieri [a,b], Thomas Blank [c], Jochen Kriegseis [a,*]

*a*Institute for Fluid Mechanics (ISTM), Karlsruhe Institute of Technology (KIT), Kaiserstr. 10, Karlsruhe, 76131, Germany
*b*Department of Mechanical and Aerospace Engineering, Politecnico di Torino, Corso Duca degli Abruzzi 24, Torino, 10129, Italy
*c*Institute for Data Processing and Electronics (IPE), Karlsruhe Institute of Technology (KIT), Hermann-von-Helmholtz-Platz 1, Eggenstein-Leopoldshafen, 76344, Germany

Abstract

In the current experimental investigation various electrode and dielectric materials for dielectric-barrier discharge plasma actuators have been studied in quiescent air under consideration of actuator degradation during long-term operation. The performance variation of the different actuators was initially monitored via alteration of the electrical power consumption $\bar{P}_a$ during 6-hour continuous operation. While some material combinations led to premature failure, certain dielectrics such as quartz-glass and aluminum oxide maintained constant performance. The latter was selected for screen-printing of electrodes, so as to obtain reproducible actuator geometries. These actuators were deployed in 10-hour continuous operation. Besides $\bar{P}_a$, the cold capacitance C_0 was tracked for each actuator, in order to assess the degradation process of the actuator. Among the tested metals for the screen-printed electrodes, copper showed the best endurance characteristics and, thus, is recommended for both comparable laboratory experiments and durability in AFC application. Admixtures of platinum in the electrode material are to be avoided because of heavy oxidation under ozone exposure. The quantitative outcomes supported by the $\bar{P}_a$ and C_0 measurements were qualitatively supported by visual inspection of the actuators and of the discharge light emission. On a final note, the screen-printed copper-aluminum-oxide actuator configuration, featuring both good durability and reproducibility, is a recommended combination.

Keywords: dielectric barrier discharge, plasma actuator, material degradation, actuator performance

1. Introduction

In recent decades, dielectric barrier discharge (DBD) plasma actuators (PAs) have received great attention in the field of fluid mechanics, as they generate an ionic wind exploited for active flow control (AFC) on aerodynamic surfaces [6, 10, 11]. A variety of applications of these devices like e.g. flow-circulation control, control of flow instabilities and conditioning of turbulent flow friction drag has been considered so far [12, 30]. Both simple design and a broad range of operational forcing parameters render PAs unique when inducing a wall jet without moving parts [10, 22].

Typically, DBD PAs are comprised of two electrodes, separated by a dielectric layer, as shown in Figure 1. One electrode is encapsulated by an insulation and the other one is air-exposed. An alternate-current (AC) high voltage (HV) in the lower kHz-range is applied between the electrodes, which induces a gas discharge from the exposed electrode onto the dielectric above the encapsulated electrode. The resulting charges are accelerated and, by collisions with neutral particles, they transfer momentum to the surrounding air. Since PA application for AFC is a comparatively young branch in the field, there is ongoing progress obtained through laboratory investigations, covering the high demands for acquiring further understanding
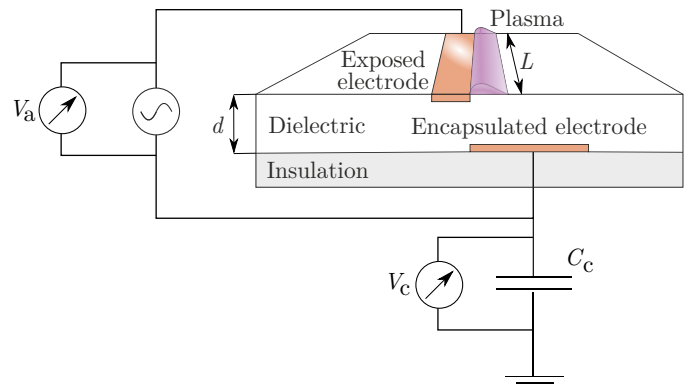

Figure 1: Schematic overview of a DBD PA and instrumentation for quantification of the electrical power consumption via the electric-charge method; the actuator voltage V_a is measured at the exposed electrode, the charge Q_a crossing the actuator is determined from the probe voltage V_c measured across a probe capacitor with capacitance C_c via $Q_a = C_c V_c$ at the encapsulated electrode.

on electrical, fluid-mechanical and performance characteristics of these actuators.

Apart from an intentional performance variation by user-adjusted operating conditions, such as e.g. voltage amplitude, plasma frequency or duty cycle, however, there are also numerous further parameters, which have demonstrated to favorably or adversely affect the control authority of PAs. Among them, the discharge intensity has shown to immediately depend on the

surrounding state variables and species such as e.g. pressure [3, 24], temperature [15, 35], humidity [4] and oxygen concentration [14]. Any changes of the surrounding ambient conditions, therefore, directly change the discharge performance, thus, AFC authority of the PA during operation. While none of the above-mentioned factors under real atmospheric conditions can be controlled, the fabrication- and material-related parameters of the PA form another group of influencing factors, controllable by the manufacturer or operator.

On the one hand, electrode or dielectric imperfections, and misalignment of the electrodes affect the discharge intensity, requiring automated manufacturing of PAs for reproducibility and homogeneity of the discharge front. Such constraints, however, also imply direct requirements for the development of a rapid prototype manufacturing routine for PA fabrication. In this context, hand-made PAs cannot fulfill such requirements, whereas they are commonly preferred for laboratory investigations due to simplicity and prompt availability. On the other hand, implications of long-term operation on the PA performance behavior are more critical. The mixture resulting from collisions is locally bipolar despite quasi-neutrality [16]. In the process, radicals are formed, ozone (O_3) in particular for operation in air [19]. Therefore, the actuator and model surface in the proximity of the forming plasma are exposed to O_3 and to other radicals. Furthermore, electron bombardment, higher temperature and ultra-violet radiation[31] contribute to the deterioration of PAs. In particular, the generated heat adversely affects the PA lifetime, increasing both dielectric and ambient temperature. The effect is, however, mitigated when the PA is exposed to an external airflow [21].

Certain dielectric materials, like e.g. Kapton (polyimide tape), indicate strong degradation, particularly under quiescent-air conditions [18]. Alternative dielectrics with higher lifetime performance were investigated by Bian *et al.* [8, 9] as combinations of Kapton and aluminum oxide (Al_2O_3)[8], and pure Al_2O_3 or aluminum nitrite (AlN)[9]. Due to dielectric degradation of Kapton, the electrical power evolution shows an increase [7, 18] and for silver (Ag) electrodes the inverse effect, enhanced by electrode oxidation, is generated [7]. Another promising study regarding the manufacturing of durable PAs has been reported by Houser *et al.* [20], where alkali-free borosilicate glass and tungsten were chosen as dielectric and electrode materials, respectively to fabricate micro-actuators by means of photolithography.

Material implications, which likewise imply actuator performance changes, are hypothesized to moreover lead to ambiguous results when interpreting and comparing fluid-mechanical characteristics recorded by different measurement techniques. As the fluid-mechanical characterization is a mandatory process in understanding the momentum-transfer capability of a new PA, such experiments are typically established in the beginning of a plasma-related research project. Knowledge on velocity information is on the one hand important to assess the flow-inducing capabilities of the actuator, e.g. for AFC, on the other hand the exerted body force as the cause of the induced flow can be derived [2, 5, 13, 23, 29, 35], e.g. for to feed numerical simulations. Depending on the applied measurement technique to gain velocity information[22], a single measurement might take a few seconds to up to several hours, so as to ensure e.g. statistical significance of the data. Therefore, PA performance is required to remain unaffected, which implies durable prototype actuators with long lifetime and constant operating properties. Beyond fluid-mechanical characterization of PAs operated under laboratory conditions, another critical requirement is long-term durability for AFC purposes. Thus, the materials used to build the actuators need to be resistant to the stresses induced on both dielectric and electrodes by any of the aforementioned phenomena.

Since rather few studies considered the long-term durability of actuator materials [7, 8, 18, 20, 32, 34], more investigations into enhanced fabrication of PAs, and alternative dielectric and electrode materials are needed. In continuation of the above efforts, the objective of the current work is to provide a reliable material combination for durable PAs suitable for long-term operation and fast manufacturing routines. More specifically, various material combinations will be considered for both hand-made and automated actuator production based on a screen-printing approach. The focus will be on monitoring the electrical PA properties, which has previously been demonstrated to be an appropriate diagnostic tool[18, 26], so as to track the PA performance over several hours of operation. The cold capacitance of the actuator[27], representing the capacitance of the passive component, will be considered as a critical measure, determining the capability of the dielectric-electrode material composition to withstand continuous plasma discharges for at least 10 hours.

2. Experimental arrangement and methodology

2.1. Plasma actuators

The PAs used in this work featured an exposed and encapsulated electrode width of 2.5 and 10 mm, respectively. The dielectric thickness of the PA varied between the different materials, as presented in Table 1, and will be indicated correspondingly.

PAs were operated with a variable HV and AC source via a HV transformer (*Minipuls 6*, GBS Elektronik GmbH) fed by a laboratory power supply (*VLP-1405 PRO*, VOLTCRAFT®). A *DSO-X 2004A* oscilloscope (Agilent Technologies Inc.) was used as wave generator to drive plasma discharges with a sinusoidal AC signal of frequency $f = 11$ kHz. To protect the PA from movements in the surrounding air, which could alter or affect the acquired velocity information, the PA was installed inside a closed box. The components of the plasma-generation system are shown in the experimental setup in Figure 2.

The PAs were either manufactured manually by hand or using screen-printing, as will be discussed in the following paragraphs.

2.1.1. Hand-made actuators

For the hand-made actuators (see Tab. 1) the widely-used Cu-Kapton (electrode-dielectric) combination for PAs is known

Table 1: Overview of investigated PA materials and related geometric dielectric and electrode dimensions.

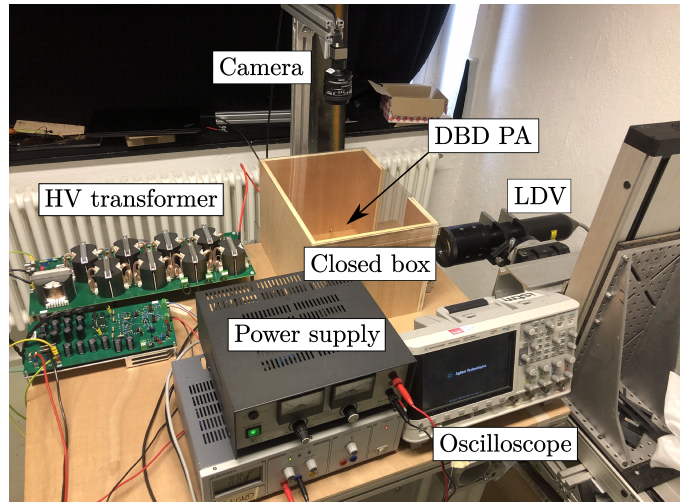| Materials		Actuator dimensions		
Electrodes	Dielectric	Dielectric thickness d (mm)	Electrode thickness d (μm)	Plasma length L (mm)
Hand-made/-painted actuators				
Cu	Kapton	0.44	50	150
Cu	Quartz glass	1.00	50	80
Cu	Al$_2$O$_3$	0.68	50	90
Paint (exp.) Cu (encpas.)	Kapton	0.44	200	80
Paint	PMMA	8.00	400	150
Paint (exp.), Cu (encaps.)	Quartz glass	1.00	300	80
Screen-printed actuators				
AgPd	Al$_2$O$_3$	0.68	20	75
AgPt	Al$_2$O$_3$	0.68	20	75
Cu	Al$_2$O$_3$	0.68	20	75

Figure 2: Experimental setup including the LDV system, a camera mounted above the PA, HV transformer, laboratory power supply and a box to protect the PA from surrounding air-flow influence.

to undergo heavy degradation in quiescent air [18]. Therefore, further electrode-dielectric combinations were tested (see Tab. 1) to evaluate the durability of hand-made actuators, as will be discussed in Section 3.1. A conductive paint was tested to achieve higher reproducibility, as paint can be filled in a machine-made groove. To ensure the general usability of this paint, three different PAs were manufactured, varying in the dielectric. For the paint-Kapton and paint-quartz glass PA the groves were hand-made using adhesive tape as edges. A more reproducible manufacturing procedure was achieved for the paint-polymethylmethacrylate (PMMA) PA, by milling a groove of the electrode geometry into the PMMA, which was subsequently filled with conductive paint by hand. To mill PMMA a certain dielectric thickness was needed. Nevertheless, PMMA is advantageous in comparison to glass as a dielectric material as it is well-machinable and was therefore considered. Instead, the benefit of the paint-glass combination is the high dielectric strength of glass as an insulator (cp. Houser *et al.* [20]). However, machining glass is more challenging due to its brittle behavior. In order to furthermore compare the quality of the applied conductive paint, a Cu-glass combination was added to the test matrix. The last tested hand-made combination was Cu–Al$_2$O$_3$; Al$_2$O$_3$ is a commonly-used dielectric [9], which exhibits rather high dielectric strength compared to quartz glass. Parasitic discharges on the lower dielectric side were avoided by attaching an insulating Kapton layer to the encapsulated electrode of all actuators.

2.1.2. Screen-printed actuators

For the automation-fabricated PAs, electrically-conductive electrodes were screen-printed on Al$_2$O$_3$ plates as dielectric. Using thick film printing, a metallic paste is applied on the dielectric. Subsequently, during the drying phase, the solvents are vaporized at a controlled temperature of 150 °C. Finally, the paste is subjected to a high-temperature treatment at 850 °C, re-

sulting in the formation of a thin adhesive layer that bonds the metal to the ceramic substrate. This standardized fabrication process creates a metal layer of 20 μm thickness with accurate repeatability properties, as required for the typical circuit-board fabrication process. In addition, an overglaze was printed onto the lower electrode, which replaces the previously used Kapton insulation. Such machine-produced insulating overglaze provides higher quality than a hand-made Kapton layer, as air pockets are completely avoided. The former are critical of inducing extra parasitic plasma discharges in unwanted locations; i.e. below the dielectric. Moreover, screen-printing of the PAs ensures reproducibility of the actuator geometry. However, the above advantages come at cost of a slightly limited choice of electrode materials. In particular, tungsten, which was proven advantageous in the study of Houser *et al.* [20], can not be processed in the thick film printing facility due to required burn-in temperature of 1800 °C. Thus, for the present study Cu (copper), AgPd (silver-palladium) and AgPt (silver-platinum) combinations (cp. Tab. 1) were applied and contrasted. A sketch of the screen-printed PA is shown in Figure 3, where the insulation is made of so-called overglaze.

2.2. Quantification strategy of the electrical power consumption

The power consumption of the PA was computed via the electric-charge method, as indicated in Figure 2, where in addition to the time-resolved actuator voltage $V_a(t)$ also the probe voltage across a probe capacitor of capacitance C_c is measured to determine the charge $Q_a(t) = C_c V_c(t)$ crossing the actuator. This method has been nicely summarized and compared to other approaches by Ashpis *et al.* [1]. Generally, the power consumption reads

$$P_a(t) = V_a(t)I_a(t) = V_a(t)\frac{\mathrm{d}Q_a(t)}{\mathrm{d}t}, \tag{1}$$

where the actuator current $I_a(t)$ has already been replaced by the time derivative of the charge signal $Q_a(t)$ at the right-hand
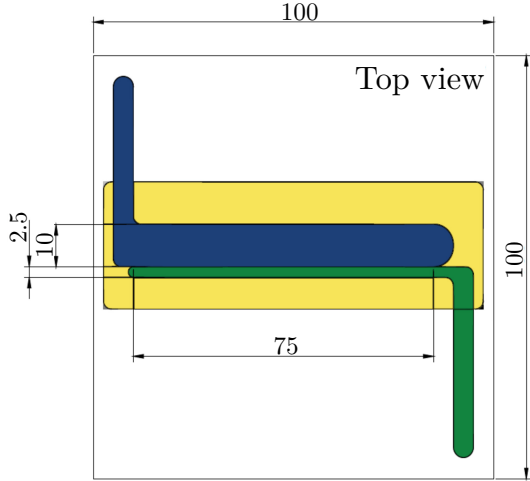
Figure 3: Screen-printed actuator with Al$_2$O$_3$ dielectric; labeled dimensions are in mm. Color code indicates dielectric (☐), overglaze (🟨) exposed (🟩) and encapsulated (🟦) electrodes

Figure 4: Lissajous curve of a DBD PA, including the effective and cold capacitances C_{eff} and C_0, respectively. The ▲-symbols show every 10$^{\text{th}}$ acquired data point.

side of Equation (1) as resulting from the chosen measurement approach. The electrical circuit representation, including all involved components is shown in Figure 1. The time-averaged power consumption per periodic discharge cycle, i.e.

$$\bar{P}_a(t) = \frac{1}{T}\int_t^{t+T} V_a(t)\frac{dQ_a(t)}{dt}dt = \frac{1}{T}\oint_T V_a dQ_a, \qquad (2)$$

is obtained through integration of Equation (1) over the period $T = 1/f$ of the plasma-discharge cycle. The result of plotting such a $Q_a - V_a$ cyclogram is a Lissajous curve, which is presented in Figure 4. The almond shape of the Lissajous curve is typical for surface DBD PA[27]. Following Equation (2), the area enclosed by the Lissajous figure over the period T is equivalent to the power consumption $\bar{P}_a$ of the PA per cycle. This method is known to be more robust against micro discharges in the current signal than other methods and, therefore, determines accurate values for the power consumption [1, 17].

Furthermore, the time-resolved capacitance $C_a(t)$ of the actuator as time-dependent load in an electric circuit, is given by the slope of the $Q_a - V_a$ cyclogram, which can be immediately calculated as.

$$C_a(t) = \frac{dQ_a(t)}{dV_a(t)}. \qquad (3)$$

Kriegseis *et al.* [27] showed that two characteristic capacitances can be revealed from this slope, which are referred to as cold capacitance C_0 and effective capacitance C_{eff}; see Figure 4. Considering a single discharge cycle, the plasma collapses when the temporal rate of change of the applied voltage is reversed; i.e. in the edges of the Lissajous curve, where $dV/dt = 0$. The slope of the $Q_a - V_a$ curve in the subsequent part is related to the cold capacitance C_0, which is representative of the passive actuator component under absence of plasma formation. The quantity C_0 is device-specific and, therefore, independent of the applied operating parameters, such as peak-
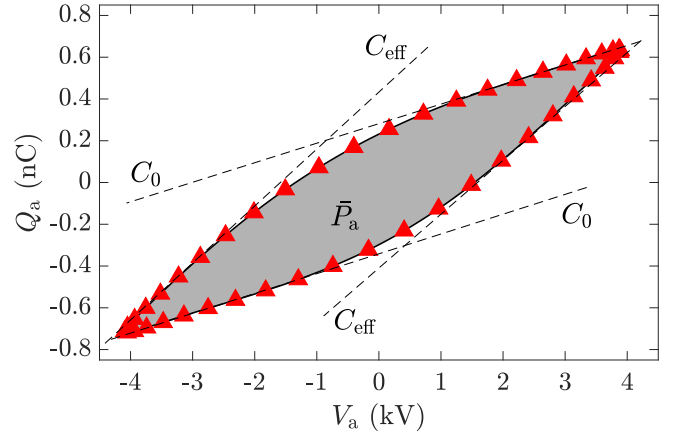
to-peak voltage V_{pp} or frequency f [27]. The effective capacitance C_{eff}, in contrast, determines the magnitude of the connected load and occurs during plasma formation, as indicated in Figure 4. To determine C_{eff} is not trivial, since the retrieved charge Q_a strongly varies. Therefore, Kriegseis *et al.* [26] used a histogram plot to identify the gradient related to both C_{eff} and C_0.

Any changes of the power consumption, imply a change of the area enclosed by the Lissajous figure, rendering either V_a or Q_a as relevant sources for a variation of the power consumption. The latter is linked to the current as shown in Equation (1). Accurate determination of V_a was ensured using a *Pintek HVP-39pro* HV probe (Pintek Electronics Co., Ltd.). For electrical data acquisition, a high-resolution PC oscilloscope (*Picoscope 4424* by Pico Technology GmbH) was deployed. The oscilloscope features a temporal and vertical bandwidth of 20 MHz and 12 bit, respectively, and a maximum sampling rate of 80 MS/s. The connected capacitor was a ceramic capacitor with a capacitance of 15 nF.

2.3. Visual inspection

The visual inspection of the actuators was carried out using both an *uEye CP* camera (IDS Imaging Development Systems GmbH) and a digital microscope. As indicated in Figure 2, the camera was deployed from top during plasma operation to show the effects on plasma light emission. Before and at the end of the tests, i.e. before and after continuous operation, respectively, the electrode quality was inspected using a digital microscope, so as to identify any structural modifications.

2.4. Validation study

For validation purposes of the applied quantification strategy for the power consumption, the PA used by Kriegseis *et al.* [29] was reproduced and characterized by both fluid-mechanical and electrical means. The geometrical dimensions for the hand-made Cu-Kapton PA are shown in Table 1. The electrodes' dimensions are identical to Section 2.1.

4
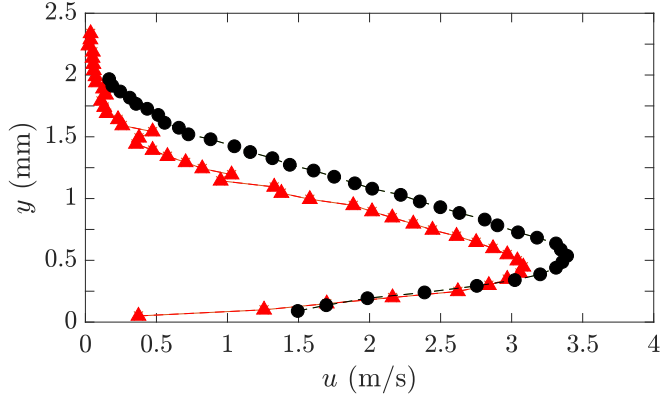
(a) Wall-normal velocity profiles $u(y)$ acquired with LDV (▲) and PIV[29] (●).
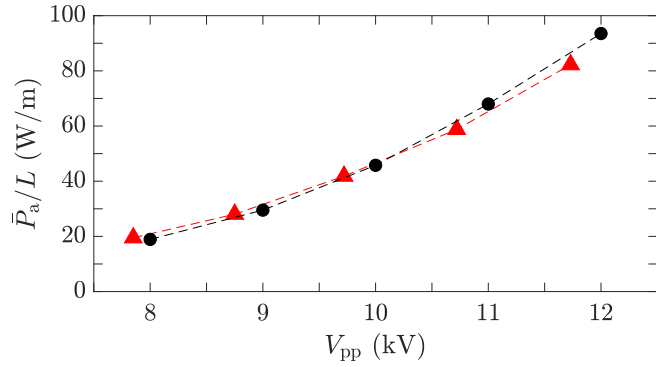
(b) Electrical power consumption P_A/L with respect to V_{pp}.

Figure 5: Electrical and fluid-mechanical characteristics of Cu-Kapton PA (see Tab. 1) in the present work (▲) compared to results of Kriegseis *et al.* [29] (●) for an identical actuator configuration.

The velocity profile was measured using a *FiberFlow* (Dantec Systems GmbH) Laser-Doppler velocimetry (LDV) device, which is a well-known measurement technique applied to small volumes as well as to obtain accurate velocity data within. The velocity data was then compared to velocity information gained through Particle Image Velocimitry (PIV)[29] for identical geometry and operating conditions; see Figure 5(a).

The resulting wall-jet velocity profile $u(y)$ measured with LDV shows comparable magnitudes in the near-wall region ($y < 0.5$ mm), while the maximum is about 10 % lower than for the PIV-acquired velocity profile by Kriegseis *et al.* [29]. Further away from the wall, the measured velocities remain smaller and show some irregularities. Since PIV is a field-measurement technique and the applied system in [29] was operated at 10 kHz repetition rate, the measurement duration is of the order of a few seconds. Instead, for LDV and other point-measurement techniques the duration can be on the order of hours, considering that the domain of interest needs to be discretized by a grid of multiple points so as to get statistically significant information across the whole field or along the wall-normal axis y as relevant for the present case of wall-jet evaluation. Accordingly, during the total measurement time of 1.5 hours for the current LDV experiments, the PA is exposed to material degradation, potentially resulting in performance changes.

In order to ensure immediate comparability of the two velocity profiles in Figure 5(a), the electrical power consumptions of the actuators used in the present LDV measurements were monitored over time and compared to those of the earlier PIV experiments[29] with identical geometry and operating conditions; see Figure 5(b). Note that the electrical quantities of the present study were acquired during the initial stages of the PA operation, i.e. when effects of possible degradation were negligible. The results show very good agreement, which confirm the operation of (initially) identical systems between the two studies.

In summary, these preliminary outcomes evidence reproducibility of the hand-made PAs, while it moreover leads to the hypothesis that degradation is deemed to play a major role in causing detrimental effects on actuator performance and durability.

3. Results and Discussion

3.1. Electrical performance I: Hand-made actuators

The power-time curves of the hand-made PAs (cp. Tab. 1) are shown in Figure 6. Note that the paint-PMMA PA is not shown in the figure, since the initially promising attemt to fabricate flush surfaced paint-flooded groove electrodes led to ran-
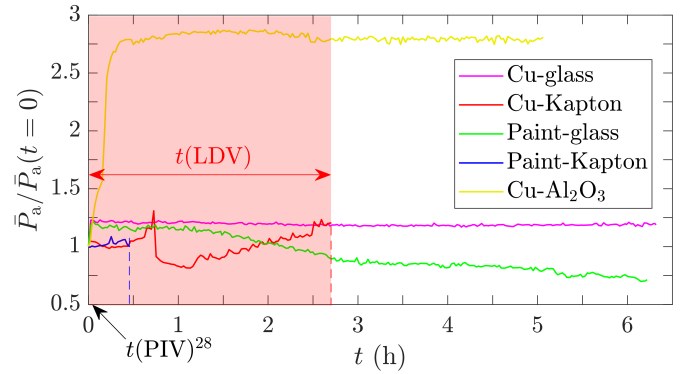
(a) $\bar{P}_a(t)/\bar{P}_a(t=0)$.
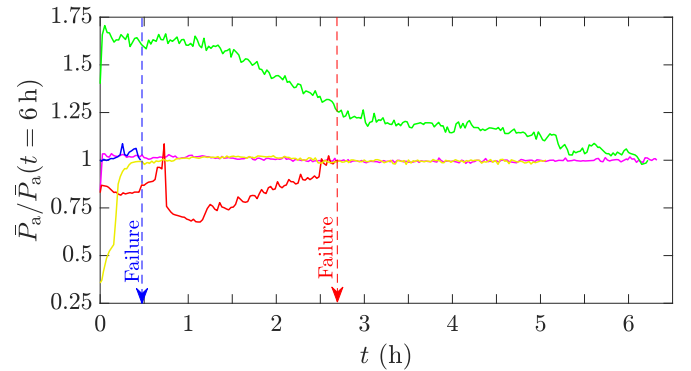
(b) $\bar{P}_a(t)/\bar{P}_a(t=6\,\mathrm{h})$.

Figure 6: Relative electrical power consumption $\bar{P}_a(t)/\bar{P}_a(t=0)$ and $\bar{P}_a(t)/\bar{P}_a(t=6\,\mathrm{h})$ of various electrode-dielectric combinations for continuous operation along a time interval of 6 hours (h).

domly distributed, inhomogeneous discharges. Since such behavior was considered an exclusion criterion for the desired flow-control applications, the paint-PMMA combination was not tested for durability but was excluded as a failed attempt.

The temporal performance behavior of the PA is represented by the relative power consumption normalized by the initial values $\bar{P}_a(t = 0)$ as also used in for the comparison with the earlier PIV results, which is shown in Figure 6(a) to emphasize the drift away from nominally (yet only initially) identical values. Furthermore, the results are also normalized with the terminate value $\bar{P}_a(t = 6\,\text{h})$ at the end of the experiment as shown in Figure 6(b). Both graphs clarify tremendous differences of the temporal progression of $\bar{P}_a(t)$. While the electrical power consumption of a PA is typically considered constant in time for continuous operation, these results evidence strong influence of degradation effects on the resulting PA power. For the paint-glass and Cu-glass combinations, the latter clearly indicates the best performance in terms of durability and temporal homogeneity. The electrical power for the paint-glass combination decreases over time by 60 %, which in comparison to the outcomes of the Cu-glass combination is attributed to the reducing conductivity of the paint. The worst performance is provided by the paint-Kapton and Cu-Kapton combinations giving device failure after half an hour and < 3 h, respectively. In agreement with earlier reports by Hanson *et al.* [18], the observed early failure has been found to result from the degradation of the Kapton dielectric.

The underlying erosion of the dielectric can be clearly seen in the marked-up region (turquoise dash) of the visualization of Figure 7, where plasma formation occurred.

For the Cu-Al$_2$O$_3$ combination, the actuator performance is similar to that of the Cu-glass combination. However, the Al$_2$O$_3$ dielectric seems to require some initial operation runtime during which the electrical power increases consistently until reaching a constant plateau. On comparing the two material combinations, the Cu-glass PA takes about a few minutes to attain $\bar{P}_a(t) = $ constant, whereas for the Cu-Al$_2$O$_3$ PA such behavior sustained only after three hours of operation.

In summary, the outcomes of the measurements with the Cu-glass and the Cu-Al$_2$O$_3$ PAs prove appropriate long-term characteristics for flow-inducing actuators, where the related dielectric properties ensure durability. The applied Cu electrode strips have not revealed any visual degradation effects (cp. also Figure 7). The simplicity of hand-made manufacturing of PAs is an advantage over automated fabrication techniques for early proof-of-concept studies, for instance. However, hand-made production is not a viable approach, when PAs are considered for thorough investigations of flow-control applications, as reproducibility is not guaranteed. Therefore, automation of the fabrication procedure is required to produce both durable but more importantly reproducible PAs with identical fluid-mechanical and electrical characteristics.

3.2. Electrical performance II: Screen-printed actuators
3.2.1. Electrical performance characteristics

Reproducible screen-printed PAs (see Sec. 2.1.2) were examined under 10 hours continuous operation. The corresponding
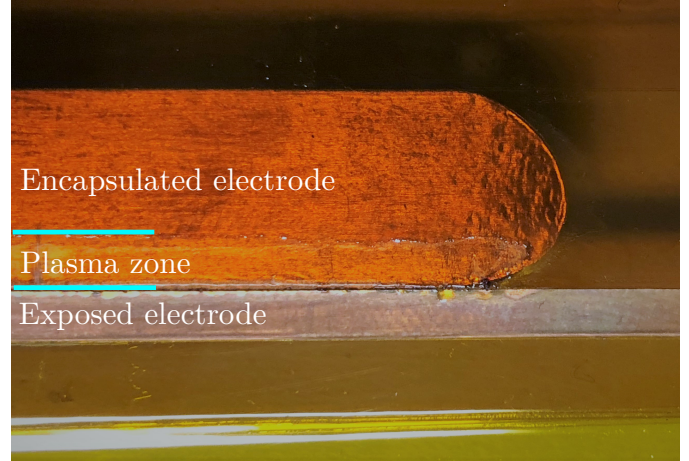

Figure 7: Degradation of the dielectric of the Cu-Kapton PA after 3 hours of operation. Dielectric degradation is visible as the brighter area in the plasma zone (——).

power- and voltage-time curves of the screen-printed PAs are shown in Figure 8. The experiments took place over the duration of two weeks during day time in a lab comprised of a central remote-controlled building ventilation system. As such, no significant changes of state variable (e.g. temperature, humidity) were expected to occur upon experimentation.

The relative electrical power consumption $\bar{P}_a(t)/\bar{P}_a(t = 4\,\text{h})$ of the PAs is depicted in Figure 8(a). As observed in Section 3.1 for the hand-made Cu-Al$_2$O$_3$ PA, normalization of $\bar{P}_a$ with the quantities at the beginning of the operation, might be in fact misleading. Accordingly, $t = 4\,\text{h}$ was chosen to the initially ($t < 4\,\text{h}$) similar pattern characteristics, for which the power drops before undergoing an increase. The identified similarity is considered a general ramp-up period of the discharge properties for the considered PAs, which obviously settles after $t \approx 4\,\text{h}$ as also seen in Figure 6. It becomes obvious from Figure 8 that the Cu-Al$_2$O$_3$ PA operates most stable for $t > 4\,\text{h}$, as $\bar{P}_a(t)/\bar{P}_a(t = 10\,\text{h})$ shows an approximately constant value with deviations below $-2.5\,\%$. In contrast, for the AgPd- and AgPt-Al$_2$O$_3$ PAs, the power drops by $> 10\,\%$. Furthermore, the overall characteristics of the power show a more stable behavior for the Cu-Al$_2$O$_3$ PA, whereas the others exhibit significant fluctuations, which is attributed to irregularities of the discharge and local charge accumulation due to electrode imperfections and degradation.

The voltage-time curves in Figure 8(b) resemble the trends of the power-time progression. For the Cu-Al$_2$O$_3$ PA, V_{pp} decreases by up to 0.5 % in the long-term run. In contrast to that, V_{pp} decreases by > 1.5 and $> 2\,\%$ for the AgPd- and AgPt-Al$_2$O$_3$ PAs, respectively.

Time-averaged Lissajous figures of the three different PAs are shown in Figure 9 at selected instances in time, so as to give an overview of the evolution of the actuator performances during operation. The positions are indicated with vertical lines in Figure 8. The cyclograms in Figure 9(a) (Cu electrode) reflect minor variations over time, which is in agreement with the

(a) Cu-Al$_2$O$_3$ PA (■).

(b) AgPd-Al$_2$O$_3$ PA (■).
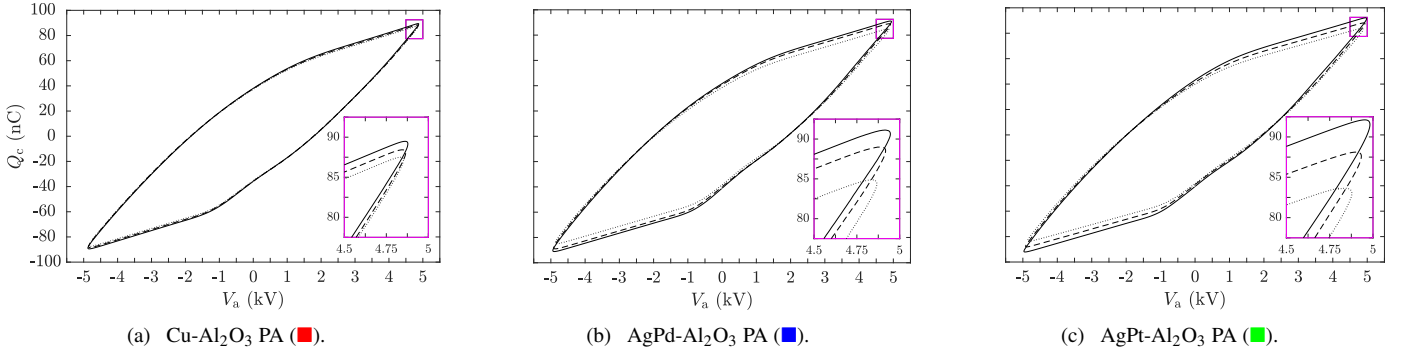
(c) AgPt-Al$_2$O$_3$ PA (■).

Figure 9: Time-averaged Lissajous figures of 500 consecutive discharge cycles for the three different PA material combinations at particular points of time within 10 h operation: —, $t = 4$ h; - - -, $t = 7$ h; $\cdots$, $t = 10$ h. Positions indicated in Figure 8. These are indicated by identical linestyles in Figure 8). The inset (□) shows a zoomed-in view of the corners. Identical color coding as used for the different materials in Figure 8 are indicated in the subfigure captions.

corresponding power-time curve in Figure 8(a). Notable differences of charge Q_c are observed in Figure 9(b) and 9(c) (AgPd and AgPt electrodes, respectively), as further emphasized by the insets (□) in the diagrams. Due to the compression of the abscissa in Figure 9, the small changes of voltage remain undetected. While the progression of the electrical power can be par-
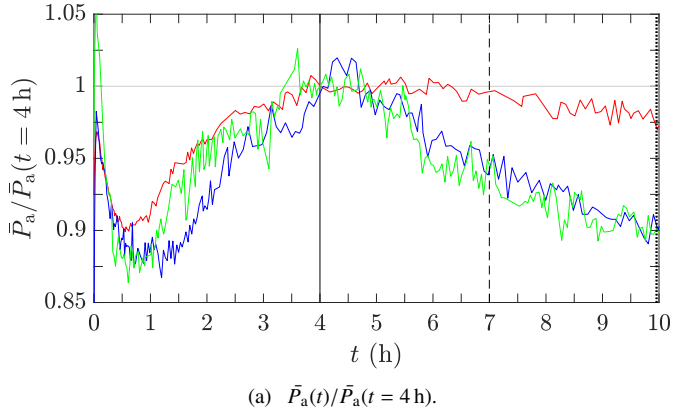
(a) $\bar{P}_a(t)/\bar{P}_a(t = 4\,\text{h})$.
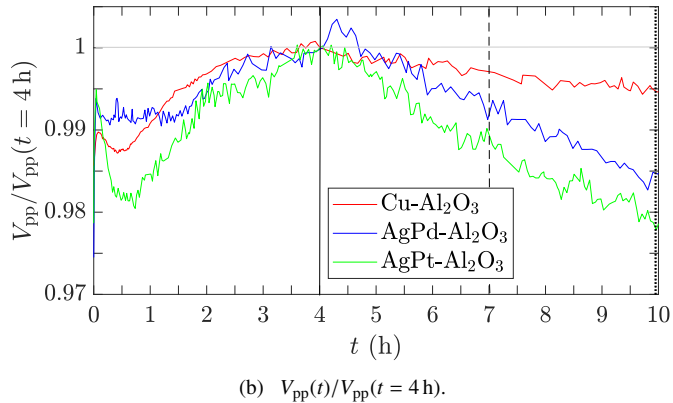
(b) $V_{pp}(t)/V_{pp}(t = 4\,\text{h})$.

Figure 8: Relative electrical power consumption $\bar{P}_a(t)/\bar{P}_a(t = 4\,\text{h})$ and peak-to-peak voltage $V_{pp}(t)/V_{pp}(t = 4\,\text{h})$ of various electrode-dielectric combinations for continuous operation along a time interval of 10 h. Vertical lines indicate time instances as used for further evaluation of the Lissajous shape; see Figure 9 and corresponding discussion.

tially referred to likewise changes of V_{pp} and identified changes of Q_c, these measures contain no information on durability in terms of degradation. Any PA degradation is instead monitored via variations of C_0, representing the passive component of the PA.

Therefore, results of the relative cold capacitances $C_0(t)/C_0(t = 0)$ for the various electrode materials are shown in Figure 10. Variation of C_0 implies a modification of capacitance of the passive component of the PA, which is obviously requested to remain constant for constant material and geometry conditions. Clearly, C_0 decreases by about only 1 % during the 10-hour operation of the Cu-Al$_2$O$_3$ and AgPd-Al$_2$O$_3$ PAs. In contrast, a significant degradation is observed for the AgPt-Al$_2$O$_3$ PA, which is reflected in a monotonous drop of C_0 by > 8 % within in 10-hour time interval.

3.2.2. Visual electrode inspection

The identified material degradation via C_0 in Figure 10 for the screen-printed PAs is further analyzed by visual inspection of the actuators in the following. While the Al$_2$O$_3$-dielectric remained optically undamaged, the electrodes were heavily attacked by the induced plasma species. The erosion of electrodes over time is shown in Figure 11 for the AgPd-electrode. The
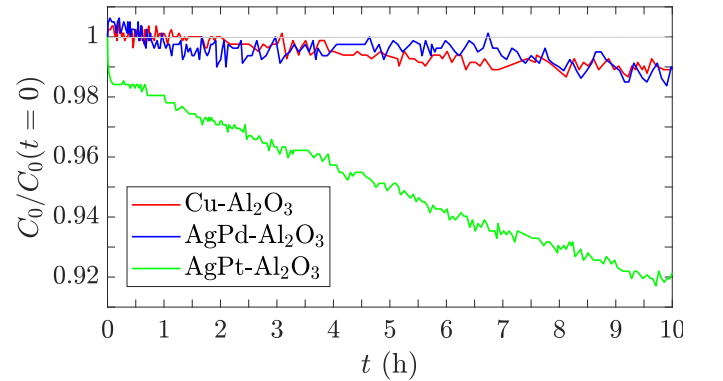

Figure 10: Relative cold capacitance $C_0(t)/C_0(t = 0)$ of the various electrode-dielectric combinations for continuous operation along a time interval of 10 h as indicator for the temporal evolution of the actuator-material properties.
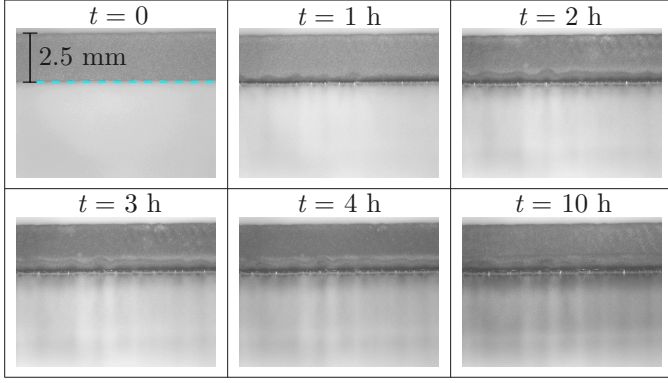
7

Figure 11: Electrode degradation of the AgPd-Al$_2$O$_3$ PA after various t. Plasma-facing edge of the exposed electrode is indicated (- - -) in the first image ($t = 0$) for orientation purposes.

strongest modification is observed for $0 \leq t \leq 1\,$h as a blackening of the discharge-generating electrode edge. Moreover, some dark streaks appear on the dielectric in regions of pronounced discharges.

Higher-resolution images of the electrodes are shown in Figure 12 as a before- vs. after-10-hour operation comparison for all electrode-dielectric material combinations. The Cu-electrode reveals a greenish to bluish oxidation layer, while the shape of the discharge-generating edge after 10-hour operation remains identical as compared to before operation. In contrast, the AgPd-electrode shows certain degree of blackening and deformation of the electrode shape after 10-hour operation. The AgPt-electrode undergoes the heaviest impact by the plasma discharge and the corresponding occurrence of ozone O$_3$ species. The entire discharge-generating edge vanishes and the original electrode shape becomes unrecognizable. Selivonin *et al.* [34] found in similar experiments that the blackened electrode edge represents a layer of oxidized electrode material. In continuation of this earlier report, the present results indicate the level of electrode oxidation to scale with the metal characteristics. Among the applied metals, the positive standard potential E_{H_2} based on hydrogen (H$_2$) classifies all of them as precious metals. The higher E_{H_2}, the more precious the metal, where E_{H_2} for Cu, Ag, Pd and Pt is 0.35, 0.8, 0.85 and 1.5 V.
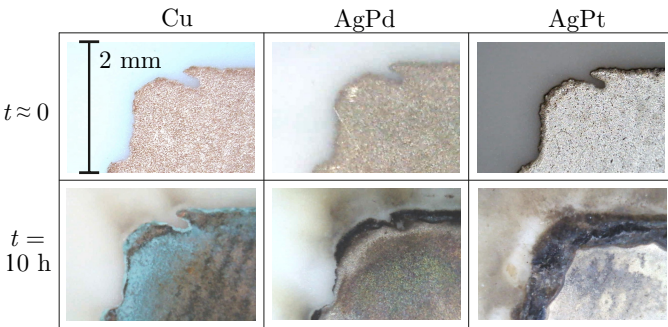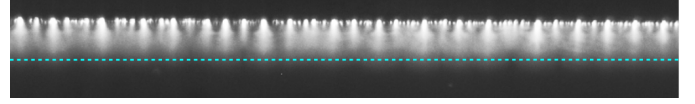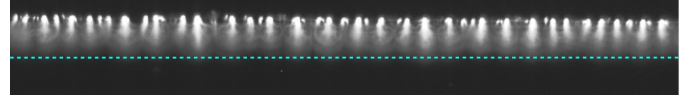

Figure 12: Zoomed-in view images of exposed electrodes for the various electrode-dielectric combinations. Comparison of electrodes initially and for $t = 10\,$h of continuous operation.
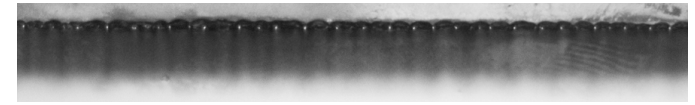

(a) Light emission at the start of 10-hour operation.

(b) Light emission after 10-hour operation.

(c) Subtraction of (b) from (a). Color code from Black, indicating no differences, to white, showing decreased light intensity.

(d) Electrode visual inspection after 10-hour operation.

Figure 13: Plasma light emission and electrode degradation of AgPt-Al$_2$O$_3$ PA. The turquoise dashed line clarifies the decrease of light-emission intensity over time.

Particularly Pt – the most precious among the applied metals – is known to oxidize well under O$_3$ treatment[33]. Even though the amount of contained Pd and Pt is less than 15 %, the admixture of Pt appears to have a strong effect in terms of oxidation characteristics, which also leaves a footprint on the C_0 development of the actuator (cp. Figure 10).

The authors of [34] further showed that the oxidation layer also affects the position of plasma micro-discharges. In general, a homogeneous appearance of the discharge pattern along the electrode with less distinct single micro-discharges is of advantage to achieve a homogeneous (independent of the space coordinate along the electrode) induced wall-jet. Single distinctive plasma discharges lead to local charge accumulation and increase of electrical power, causing stronger discharge events. These can be visually monitored by light-emission analysis. Local charge accumulation directly affects the requested spatial homogeneity of the plasma-induced flow field.

Results of light-emission discharge analysis are shown in Figure 13 for the AgPt-Al$_2$O$_3$ PA. The total light emission at the start of the 10 h operation is strong and rather homogeneously-distributed along the electrode edge; see Figure 13(a). In contrast, only very distinctive, local plasma discharges occur after 10-hour operation as shown in Figure 13(b), indicating the effect of the oxidation layer[34] and, moreover, electrode degradation (cp. Figure 10). Furthermore, the overall light intensity decreases as supported by the turquoise dashed line in Figure 13(a) and 13(b). This effect is further emphasized through subtraction of both images from each other, which is shown in Figure 13(c). The oxidation layer, presented in Figure 13(d), exhibits a wave-like pattern, which can be associated with the location of occurring plasma discharges in Figure 13(b).
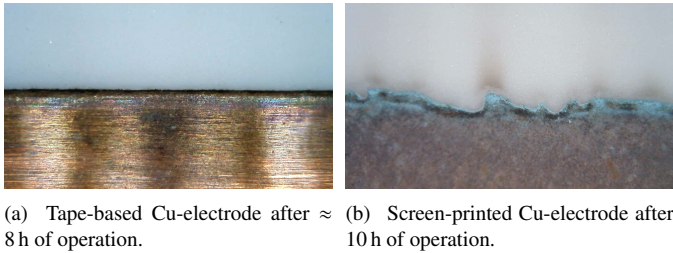
(a) Tape-based Cu-electrode after $\approx$ 8 h of operation.

(b) Screen-printed Cu-electrode after 10 h of operation.

Figure 14: Comparison of oxidation effects on the exposed Cu-electrode edges for differently fabricated Cu-Al$_2$O$_3$ actuators.

The effect of electrode-edge imperfections of screen-printed PAs on the observed oxidation was *a posteriori* considered by comparing the former with the tape-based Cu-Al$_2$O$_3$ PA as discussed in Section 3.1. A direct comparison of actuators is provided in Figure 14. The Cu-tape-based PA as shown in Figure 14(a) reveals minor blackening very close to the electrode edge. Furthermore, the edge quality is better when compared to the screen-printed electrode in Figure 14(b). The hereby increased surface area due to the torn pattern of the electrode edge could play a major role for the electrode oxidation. In other words, increased stresses due to the poor edge quality, enhance degradation caused by local charge accumulation on the existing spikes.

4. Concluding remarks

The current work addresses the degradation of dielectric and electrodes during long-term testing of DBD PAs, which represents a critical aspect towards both comparable laboratory experiments and viable AFC application. For the former, any performance changes of the PA due to degradation immediately influence the outcomes of experimental studies as an immediate result from the different device-specific measurement durations. Considering instead in-flight continuous PA operation, the optimum AFC conditions cannot be guaranteed under degrading discharge performance and accordingly changing or even unpredictable controller characteristics [25].

Generally, the electrical power consumption gives evidence about performance changes. However, in order to distinguish the origin of such changes between environmental influences and the degradation process of the actuator itself, the most important monitoring parameter is the cold capacitance C_0 [18, 28]. Therefore, continuous monitoring of the electrical quantities Q_a and V_a is recommended to keep track of performance changes through actuator degradation via C_0.

As a major step towards durable electrode-dielectric combinations for PAs, a screen-printing technique delivered a durable actuator configuration, which remained rather unaffected by degradation processes imposed through O$_3$, electron bombardment and temperature effects. The fabrication procedure allowed for reproducible electrode geometries on an Al$_2$O$_3$ dielectric, which is a beneficial complement to the already existing robust fabrication approach of tungsten/glass actuators based on photolitography as reported by Houser et al. [20]. As

for the presented screen-printing technique, future steps might aim at the perfection of the electrode edge quality (cp. Fig. 12 for $t \approx 0$) and correspondingly optimized discharge quality.

For the investigated screen-printed PAs, electrode degradation appeared more critical than dielectric degradation. The presented proof-of-concept study regarding the chosen fabrication process clearly demonstrated that the most durable considered electrode material was Cu. For more precious materials such as mixtures of Ag and Pd, and Ag and Pt, significant oxidation layers were found after 10-hour operation. It has to be consequently concluded from the achieved insights that, due to the oxidation properties of Pt under O$_3$ exposition [33], any admixture of Pt in the electrode material should be avoided. This salient material-specific trend might be subject to future quantification studies to cross-check the accuracy of the standardized fabrication process from the perspective of dielectric barrier discharges, where the latter is usually particularly avoided during circuit-board design.

In summary, the study emphasizes the importance of continuously tracking actuator performance characteristics, and as an outcome of the experiments, provides a durable, reliable and reproducible DBD-PA configuration. On that account, both comparability of future laboratory tests can be ensured under unaltered ambient conditions and the assessment of further performance-influencing quantities, such as e.g. environmental state variables and/or airflow encounter can be assessed independent from both possible actuator degradation and chosen diagnostics equipment for the performance evaluation.

References

[1] Ashpis, D.E., Laun, M.C., Griebeler, E.L., 2017. Progress toward accurate measurement of dielectric barrier discharge plasma actuator power. AIAA J. 55, 2254–2268. doi:https://doi.org/10.2514/1.J055816.

[2] Baughn, J., Porter, C., Peterson, B., McLaughlin, T., Enloe, C., Font, G., Baird, C., 2006. Momentum transfer for an aerodynamic plasma actuator with an imposed boundary layer. AIAA paper 2006-168. doi:https://doi.org/10.2514/6.2006-168.

[3] Benard, N., Balcon, N., Moreau, E., 2008. Electric wind produced by a single dielectric barrier discharge actuator operating in atmospheric flight conditions – pressure outcome. AIAA paper 2008-3792. doi:https://doi.org/10.2514/6.2008-3792.

[4] Benard, N., Balcon, N., Moreau, E., 2009. Electric wind produced by a surface dielectric barrier discharge operating over a wide range of relative humidity. AIAA paper 2009-488. doi:https://doi.org/10.2514/6.2009-488.

[5] Benard, N., Debien, A., Moreau, E., 2013. Time-dependent volume force produced by a non-thermal plasma actuator from experimental velocity field. J. Phys. D: Appl. Phys. 46, 245201. doi:https://dx.doi.org/10.1088/0022-3727/46/24/245201.

[6] Benard, N., Moreau, E., 2014. Electrical and mechanical characteristics of surface ac dielectric barrier discharge plasma actuators applied to airflow control. Exp. Fluids 55. doi:http://dx.doi.org/10.1007/s00348-014-1846-x.

[7] Bian, D., Wu, Y., Long, C., Lin, B., 2018. Effects of material degradation on electrical and optical characteristics of surface dielectric barrier discharge. J. Appl. Phys. 124, 183301. doi:https://doi.org/10.1063/1.5049463.

[8] Bian, D.L., Wu, Y., Jia, M., Long, C.B., 2017a. Pi/al2o3 nanocomposite based long lifetime surface dielectric barrier discharge plasma actuator. Sens. Actuator A Phys. 267, 90–98. doi:https://doi.org/10.1016/j.sna.2017.10.008.

[9] Bian, D.L., Wu, Y., Jia, M., Long, C.B., Jiao, S.B., 2017b. Comparison between aln and al2o3 ceramics applied to barrier dielectric of plasma actuator. Chin. Phys. B 26, 084703. doi:https://dx.doi.org/10.1088/1674-1056/26/8/084703.

[10] Cattafesta, L.N., Sheplak, M., 2011. Actuators for Active Flow Control. Annu. Rev. Fluid Mech. 43, 247–272. doi:https://doi.org/10.1146/annurev-fluid-122109-160634.

[11] Corke, T.C., Enloe, C.L., Wilkinson, S.P., 2010. Dielectric barrier discharge plasma actuators for flow control. Annu. Rev. Fluid Mech. 42, 505–529. doi:https://doi.org/10.1146/annurev-fluid-121108-145550.

[12] Corke, T.C., Thomas, F.O., 2018. Active and passive turbulent boundary-layer drag reduction. AIAA J. 56, 3835–3847. doi:https://doi.org/10.2514/1.J056949.

[13] Debien, A., Benard, N., David, L., Moreau, E., 2012. Unsteady aspect of the electrohydrodynamic force produced by surface dielectric barrier discharge actuators. Appl. Phys. Lett. 100, 013901. doi:https://doi.org/10.1063/1.3674308.

[14] Dubois, D., Merbahi, N., Eichwald, O., Yousfi, M., Benhenni, M., 2007. Electrical analysis of positive corona discharge in airand n2,o2, and co2 mixtures. J. Appl. Phys. 101, 053304. doi:https://doi.org/10.1063/1.2464191.

[15] Erfani, R., Zare-Behtash, H., Kontis, K., 2012. Plasma actuator: Influence of dielectric surface temperature. Exp. Therm. Fluid Sci. 42, 258–264. doi:https://doi.org/10.1016/j.expthermflusci.2012.04.023.

[16] Goldston, R.J., Rutherford, P.H., 1995. Introduction to Plasma Physics. CRC Press. doi:https://doi.org/10.1201/9780367806958.

[17] Grundmann, S., Tropea, C., 2009. Experimental damping of boundary-layer oscillations using dbd plasma actuators. Int. J. Heat Fluid Flow 30, 394–402. doi:https://doi.org/10.1016/j.ijheatfluidflow.2009.03.004.

[18] Hanson, R.E., Houser, N.M., Lavoie, P., 2014. Dielectric material degradation monitoring of dielectric barrier discharge plasma actuators. J. Appl. Phys. 115, 043301. doi:https://doi.org/10.1063/1.4862309.

[19] Hong, D., Rabat, H., Bauchire, J.M., Chang, M.B., 2014. Measurement of ozone production in non-thermal plasma actuator using surface dielectric barrier discharge. Plasma Chem. Plasma Process. 34, 887–897. doi:https://doi.org/10.1007/s11090-014-9527-3.

[20] Houser, N., Gimeno, L., Hanson, R., Goldhawk, T., Simpson, T., Lavoie, P., 2013. Microfabrication of dielectric barrier discharge plasma actuators for flow control. Sensors and Actuators A: Physical 201, 101–104. doi:https://doi.org/10.1016/j.sna.2013.06.005.

[21] Joussot, R., Hong, D., Rabat, H., Boucinha, V., Weber-Rozenbaum, R., Leroy-Chesneau, A., 2010. Thermal characterization of a dbd plasma actuator: Dielectric temperature measurements using infrared thermography. AIAA paper 2010-5102. doi:https://doi.org/10.2514/6.2010-5102.

[22] Kotsonis, M., 2015. Diagnostics for characterisation of plasma actuators. Meas. Sci. Technol. 26, 092001. doi:https://doi.org/10.1088/0957-0233/26/9/092001.

[23] Kotsonis, M., Ghaemi, S., Veldhuis, L., Scarano, F., 2011. Measurement of the body force field of plasma actuators. J. Phys. D: Appl. Phys. 44, 045204. doi:https://dx.doi.org/10.1088/0022-3727/44/4/045204.

[24] Kriegseis, J., Barckmann, K., Frey, J., Tropea, C., Grundmann, S., 2014. Competition between pressure effects and airflow influence for the performance of plasma actuators. Phys. Plasmas 21, 053511. doi:https://doi.org/10.1063/1.4880098.

[25] Kriegseis, J., Duchmann, A., Tropea, C., Grundmann, S., 2013a. On the classification of dielectric barrier discharge plasma actuators: A comprehensive performance evaluation study. J. Appl. Phys. 114, 053301. doi:https://doi.org/10.1063/1.4817366.

[26] Kriegseis, J., Grundmann, S., Tropea, C., 2011a. Power consumption, discharge capacitance and light emission as measures for thrust production of dielectric barrier discharge plasma actuators. Journal of Applied Physics doi:https://doi.org/10.1063/1.3603030.

[27] Kriegseis, J., Möller, B., Grundmann, S., Tropea, C., 2011b. Capacitance and power consumption quantification of dielectric barrier discharge (dbd) plasma actuators. J. Electrostat. 69, 302–312. doi:https://doi.org/10.1016/j.elstat.2011.04.007.

[28] Kriegseis, J., Schröter, D., Barckmann, K., Duchmann, A., Tropea, C., Grundmann, S., 2013b. Closed-loop performance control of dielectric-barrier-discharge plasma actuators. AIAA J. 51, 961–967. doi:https://doi.org/10.2514/1.J052159.

[29] Kriegseis, J., Schwarz, C., Tropea, C., Grundmann, S., 2013c. Velocity-information-based force-term estimation of dielectric-barrier discharge plasma actuators. J. Phys. D: Appl. Phys. 46, 055202. doi:https://doi.org/10.1088/0022-3727/46/5/055202.

[30] Kriegseis, J., Simon, B., Grundmann, S., 2016. Towards in-flight applications? a review on dielectric barrier discharge-based boundary-layer control. Appl. Mech. Rev. 68, 020802. doi:http://dx.doi.org/10.1115/1.4033570.

[31] Pons, J., Oukacine, L., Moreau, E., Tatibouët, J.M., 2008. Observation of dielectric degradation after surface dielectric barrier discharge operation in air at atmospheric pressure. IEEE Trans. Plasma Sci. 36. doi:https://doi.org/10.1109/tps.2008.926856.

[32] Rodrigues, F.F., Pascoa, J.C., 2020. Implementation of stair-shaped dielectric layers in micro- and macroplasma actuators for increased efficiency and lifetime. J. Fluids Eng. 142, 104502. doi:https://doi.org/10.1115/1.4047800.

[33] Saliba, N., Tsai, Y.L., Panja, C., Koel, B.E., 1999. Oxidation of pt (111) by ozone (o3) under uhv conditions. Surf. Sci. 419, 79–88. doi:https://doi.org/10.1016/S0039-6028(98)00667-0.

[34] Selivonin, I.V., Lazukin, A.V., Moralev, I.A., Krivov, S.A., 2018. Effect of electrode degradation on the electrical characteristics of surface dielectric barrier discharge. Plasma Sources Sci. Technol. 27, 085003. doi:https://dx.doi.org/10.1088/1361-6595/aacbf5.

[35] Versailles, P., Gingras-Gosselin, V., Vo, H.D., 2010. Impact of pressure and temperature on the performance of plasma actuators. AIAA J. 48, 859–863. doi:https://doi.org/10.2514/1.43852.